Al-Khwarizmi Engineering Journal
ISSN (printed): 1818 – 1171, ISSN (online): 2312 – 0789
Vol. 22, No. 1, March, (2026), pp. 55- 73

Al-Khwarizmi Engineering Journal

# Design of a Compact Broadband Metamaterial Absorber with Wide-Angle Reception and Polarization-Insensitive for Electromagnetic Energy Harvesting in Wireless Sensor Network Applications

**Zainalabdin K. Flaih [1]*, Yahyaa A. Lfta[2]**
[1,2] *Department of Electronic and Communications Engineering, Faculty of Engineering, University of Kufa, Najaf, Iraq*
*Corresponding Author's Email: zainalabdink.alchallaby@student.uokufa.edu.iq

(Received 19 July 2025; Revised 1 November 2025; Accepted 24 December 2025; Published 1 March 2026)
https://doi.org/10.22153/kej.2026.12.014

## Abstract

This work introduces a novel design of a compact broadband metamaterial (MM) absorber with polarization-insensitive, wide-angle reception for ambient electromagnetic (EM) power harvesting applications. The proposed MM unit cell consists of two layers of low-cost FR-4 substrate. The top layer contains a resonator structure and four lumped resistors. A copper sheet, serving as a ground plane, is placed on the backside of the bottom layer to reduce transmission losses. The top and bottom layers are separated by a thin air layer to enhance absorption at operational frequencies. The overall size of the MM unit cell is 12×12×4.57 mm³, with measurements of 0.16λ₀×0.16λ₀×0.06λ₀ at the lowest frequency in the absorption spectrum. The unit cell's input impedance is carefully engineered to align with that of free space, an approach facilitating efficient EM power absorption and suitable redirection to resistive loads. The absorber's performance is assessed for different polarization and incident angles for transverse electric (TE) and transverse magnetic (TM) modes. The simulation results indicate that the introduced absorber attains broadband absorption, surpassing 90% in the frequency range of 4 GHz to 7 GHz. Moreover, the MM unit cell achieves harvesting efficiency above 80% under normal incidence and continues to exhibit outstanding performance over different incidence angles for the TE and TM modes. This study substantially improves MM-based energy harvesting through integrating wide-angle reception, high-absorption broadband, compact size, and polarization insensitivity, which make it an ideal option for supplying energy to wireless sensor networks.

***Keywords:*** *Broadband; Metamaterial absorber; Polarization-insensitive; RF electromagnetic energy harvesting; Wide-angle reception; Wireless sensor network (WSN)*

## 1. Introduction

Wireless communications (WCs) have become more critical, play a vital role in modern technology, and dramatically change how humans connect or interact with their surroundings. Technological advancements in WCs have been driven by wireless sensor networks (WSN)s. They have remarkably eased the integration of WCs across various areas of our daily existence [1]. Nowadays, WSNs are applied in various environmental, health monitoring, industrial, N-park monitoring, and security sectors. WSNs hold high potential for use in healthcare, where sensor nodes embedded in wearable and implantable devices can be used to track vital signs, including blood pressure, oxygen saturation, heart pulses, and electrocardiogram readings, in at-risk persons [2]. Sensor networks are increasingly helpful for the industrial branch and facilitate gathering of data regarding machinery, processes, and human–machine interaction. In addition, the simplicity of WSN deployment in industrial environments has contributed to simplifying factory infrastructure and improving reliability to achieve smart manufacturing and sustainability, which are emerging as crucial elements of the fourth industrial revolution

(Industry 4.0) [3]. WSNs should be self-sufficient, maintain continuous functionality, and necessitate less maintenance, which may be expensive and cumbersome. Consequently, a substantial demand exists for sustainable sources of power to improve energy efficiency in WSNs. Great advancements and enhancements in low-power devices, protocols of communications, software, and compact electronic devices help boost the expected lifespan and energy efficiency in sensor nodes. However, energy supply is still a major problem due to continued dependence on conventional batteries [4]. Electronic devices powered by traditional batteries typically require recharging or replacement, which presents restrictions associated with safety and environmental considerations [5]. Thus, researchers are motivated to look for new ways to generate adequate power to keep electronic devices operating continuously [6].

In the last years, researchers and scientists have explored energy harvesting approach as a viable solution to avoid challenges related to batteries and to enable sustainability. Energy harvesting denotes the collection and storage of ambient energy from outside sources, such as thermal energy from mechanical loads, solar energy from light, kinetic energy derived vibrations, and electromagnetic (EM) energy from radio frequency (RF) waves. Energy harvesting techniques utilize a specific source depending on the application-specific energy requirements and environmental conditions [7]. Radio frequency energy harvesting (RFEH) is highly attractive for low-power electronic devices and WSNs due to their availability in indoor environments [8]. RFEH refers to gathering incident EM wave energy from ambient sources and converting it into electrical energy. Ambient sources can be provided by multiple RF broadcasting infrastructures such as Wi-Fi and GSM networks. Moreover, 5G technology is coming with widespread deployment for low-power devices, such as Internet of Things (IoT) devices and sensors facilitate the explosive expansion of wireless networks, base stations of mobile communication, and other radio transmission equipment that are surrounded by rich EM energy [9], which means providing abundant RF energy in the surrounding environments.

The primary device for harvesting RF energy in an RFEH system is the rectifier antenna (rectenna) that captures EM waves by using a receiving antenna and converts the absorbed power to DC current by using a rectifier. The antenna is the main device for maximizing power harvesting. The traditional antennas used in energy harvesting have some constraints, such as low efficiency and large size [10], [11]. In addition, the energy harvested by a single antenna is minimal. Thus, the antenna array approach is recommended in numerous research to receive large amounts of power [12]. At the same time, the conventional receiving antenna arrays are constrained by their substantial dimensions, the spacing between array elements, and poor conversion efficiency resulting from mutual coupling among the array components [13]. By contrast, metasurface (MS) structures have arisen as a potential alternative to traditional rectennas. MS is a 2D MM structure that offers remarkable benefits, such as minimizing the overall collector dimensions, increasing the amount of power generation, and enhancing efficiency at the initial stage of RF to AC power [14].

MMs can be described as artificial structures with unique EM properties not found in natural materials, such as negative permeability, permittivity, and refractive index [15]. Due to the superior properties of MMs, they are used in various applications, such as antenna design, invisibility cloaking, wireless power transfer (WPT), super lenses, energy harvesting, and particularly perfect absorption of EM waves. The MM perfect absorber is considered one of the basic applications of MMs and was shown first by Landy [16], which proved the ability of the MM structure to absorb EM waves with near-unity absorbance and minimal reflection, transmission, and scattering. MM absorbers are thin structures with subwavelength dimensions. Due to the MM structures' high flexibility and light weight, they are simple to integrate into current electronic devices and systems. Consequently, these absorbers can be customized to suit the demands of specific applications [17]. The unique properties of MM absorbers are being used in many various applications. For example, MM absorbers have been utilized in the sensing field to develop extremely sensitive sensors that can detect the smallest changes in different environments [18]. In radar applications, they can absorb EM waves in Ku-band wavelength region and make items unidentifiable to military radar platforms [19]. In RFEH, these EM absorbers are also used to collect and transform EM energy into electrical energy [20]. MM absorber structures consist of an array of minute electrical resonators, including split ring res onators (SRR) [21], complementary split ring resonators (CSRR) [22], and electric-inductive-capacitive resonators (ELC) [23]. These structures work according to the EM resonance principle. At particular frequencies, they are allowed to absorb EM power by successfully coupling to the incoming EM wave. Furthermore, to obtain perfect absorption, the effective permeability and

permittivity of the material can be modified so that the impedance of the input will perfectly match the free space. MM harvesters and absorbers are built with the idea of perfect absorption and have great differences. Nearly all absorbed power is lost inside the structure as either dielectric or ohmic losses and appears as the heat in the functionality of absorption, while in harvesting functionality, the absorbed power by the resonators channeled to the rectifier circuit [24]. In MM harvester procedure, the input impedance of the rectifier is modeled by the resistive load, and it must be properly matched to the impedance of free space to attain greater RF-DC efficiency [25].

## 2. Related Work

Several studies in the scientific literature have investigated different MM absorber unit cells for RFEH, including single band [26], [13], dual band [27], [28], triple band [22], [29], multiband [30], and wide band [31]. MM harvesters have two essential characteristics that play a vital role in enhancing overall efficiency, namely, wide-angle reception and polarization insensitive (polarization independent) to incident waves [32]. According to these characteristics, numerous types of MM harvesters have been produced to enhance their applicability, involving multipolarization [33] [34], and wide incident angle and polarization insensitivity [35] [36].

Recently, researchers on MM absorbers have been focusing on creating unit cell structures with a broad absorption bandwidth across the EM spectrum due to the growing need for real world application. The main benefit of broadband MM absorbers that make them useful in RFEH is their capacity to absorb EM waves [37]. To expand the absorption range of the frequencies, complex structures have been employed in the construction of MMs unit cells. These methods utilized multilayer arranged structures and multiple metallic resonant structures [38]. However, these strategies have produced certain disadvantages, including increased overall thickness, issues in assembly, and the potential for separate absorption bands [39]. An additional technique for producing broadband MM absorber is using special materials, such as resistive film [40] and doped silicon materials [41]. These methods have produced certain problems, such as complex fabrication and high cost. An alternate approach to achieving a broad absorption range is using MM absorbers with electrical lumped resistors inserted between the upper metallic layer splits. These resistors introduce additional ohmic losses on the surface of the metallic layer. However, these resistors might not be enough to achieve broad absorption bandwidth. However, this difficulty can be addressed by constructing the absorber with a rubber or resilient foam layer (air gap) located between the ground plan and substrate. In [39], a wideband MM absorber was introduced with four lumped elements (resistors) to enhance the absorptivity and air layer insert between the FR4 substrate and ground plane to increase absorption bandwidth. The proposed design achieves 90% absorption rate through broad range of frequencies between 1.94 and 2.98 GHz with polarization-insensitive, wide-angle reception for the transverse electric (TE) and transverse magnetic (TM) phases. In [42], the authors proposed a broadband MM absorber utilizing a split circular ring configuration with four lumped resistors and one layer from metal–dielectric–metal for X-band applications. The proposed design achieves 90% absorption rate through a broad range of frequencies between 7.8 and 12.6 GHz under normal incidence with polarization-insensitive, wide-angle reception up to 30° for TE and TM polarization. In [43], square split ring resonator and four lumped resistors possessing identical resistance values of 560 Ω welded on the resonator with an air layer of 12 mm thickness was proposed for RFEH and WPT. The introduced design achieves 90% absorption rate through broad range of frequencies between 1.89 and 6.85 GHz with polarization insensitivity and wide-angle reception. The authors in [15] introduced a structure that achieves 90% EM absorption rate through wide range of frequencies between 12.3 and 14.8 GHz. The unit cell consists of 10 split rings separated into four segments; each segment has a metallic bar connecting the rings from one side. The proposed design exhibits polarization-insensitive properties for the TE and TM modes and achieves a high absorption ratio at an incident angle of up to 45°. In [44], the authors proposed an MS absorber for RFEH consisting of a square loop ring resonator formed by two L-shaped diagonally arranged and two smaller symmetrical L-shaped patches that work as tuning parts. The proposed design achieves 99% absorption rate through a broad range of frequencies between 6.7 and 8.25 GHz over multiple resistive load values between 100 and 500 Ω. The absorption bandwidth changes for different polarization angles, which can be the main problem in this structure.

Numerous studies have investigated MM absorber-based energy harvesting. However, their designs in this field have considerable drawbacks including large MM structures with high thickness;

this render them inappropriate for applications, where weight and size are crucial, especially in IoT networks, WSNs, and low-power electronic devices. Moreover, many exciting designs are restricted to a limited number of absorption frequency bands, which further diminishes the ability to capture energy from a wider spectrum of EM waves. In addition, many designs from past studies are sensitive to polarization, while some do not have wide-angle reception.

This paper introduces a compact, small-thickness, broadband, polarization-insensitive, and wide-angle reception MM absorber-based energy harvester. The proposed structure contains four lumped resistors integrated in a cross shape on the top side and a metal sheet on the bottom side with two FR4 substrates separated by an air layer. The simulation result indicates that the proposed absorber achieves an absorptivity of approximately 90% within the broad frequency range of 4 to 7 GHz with unit cell size of 12×12×4.57 mm³. Moreover, the introduced design has a maximum harvesting efficiency equal to 92.15% at normal incident angle. Surface current distribution, electric field, and magnetic field are investigated to understand the absorption. Absorption and harvesting efficiency for different polarization and reception angles are numerically verified for TE and TM polarization. This harvester exceeds prior designs in several crucial areas, which makes it very adaptable for real applications.

## 3. Unit Cell Design

The unit cell structure was designed and simulated using CST Studio Suite software, an efficient tool for simulating and designing EM components. The proposed MM unit cell consists of three dielectric layers, namely, top (FR4), middle (air), and bottom (FR4), as depicted in Figures 1a and 1b. The top dielectric layer of the unit cell incorporates four curves connected to one another by lumped resistors to construct the outer ring resonator while constructing the inner resonator with same outer resonator curves with four triangles instead of lumped elements; these triangles connected by cross-shaped patch have small slits, as shown in Figure 1c. The resonators are placed at 45° relative to the substrate to improve the interaction between the magnetic and electric field components, which would expand the bandwidth. In addition, the distance between the outer and inner resonators is very small (0.6 mm) to enhance coupling. An air layer is positioned between two dielectric substrates to achieve broadband with greater absorption capacity and higher harvesting efficiency. The bottom dielectric layer is covered with a metal sheet on the back side to construct the ground plan, as shown in Figure 1d. Annealed copper with a large conductivity ($5.8\times10^7$ S/m) and small thickness (0.035 mm) is used to create the resonators and ground plan. A 1.5 mm thick FR4 dielectric material is used as a substrate at the top and bottom layers with a 4.3 dielectric constant ($\epsilon_r$) and 0.0025 loss tangent (tan δ). Table 1 presents the optimized unit cell structure dimensions.

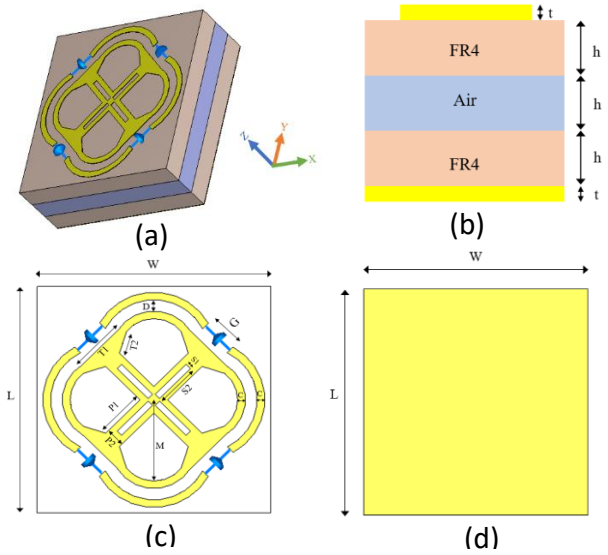


**Fig. 1. Unit cell MM absorber: (a) 3D view, (b) side view, (c) Top view, and (d) Bottom view**

The reflection coefficient ($S_{11}$) of the MM unit cell is shown in Figure 2. The structure produces reflectance below −10 dB from approximately 4 to 7 GHz at normal incidence with a relative bandwidth of a 75%. Therefore, the proposed MM absorber exhibits optimal performance between these frequencies with minimal reflection of incoming EM waves in free space.

**Table 1,**
**Optimum dimensions of the unit cell**

| Parameter | Dimension (mm) | parameter | Dimension (mm) |
|---|---|---|---|
| W | 12 | T1 | 3.17 |
| L | 12 | T2 | 1.22 |
| C | 0.4 | S1 | 0.3 |
| D | 0.6 | S2 | 2.25 |
| G | 1.8 | M | 5.3 |
| P1 | 2.5 | t | 0.035 |
| P2 | 1 | h | 1.5 |

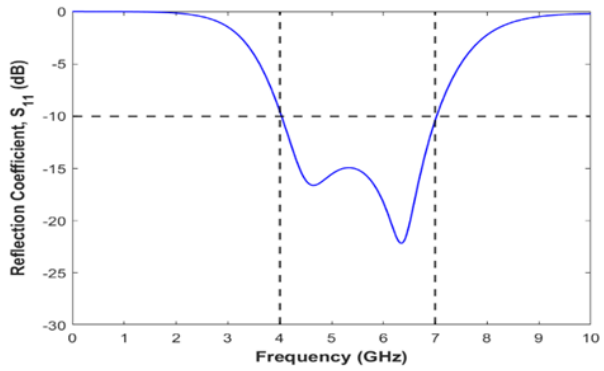


**Fig. 2. Simulated reflection coefficient ($S_{11}$) of the proposed MM absorber**

The proposed design of the top-layer resonator structure underwent a parametric study to obtain the desired resonance characteristics at the required frequencies and improve the EM wave absorption, an approach boosting energy harvesting. This analysis provided a systematic evaluation and optimization of the MM unit cell parameters. As shown in Figure 3a, four designs of unit cell resonator were evaluated, and the reflection coefficients of these designs were examined, as depicted in Figure 3b. Design 1 is composed of four curves connected by four lumped resistors with the same value (100 Ω) to form the ring resonator. The reflection coefficient of Design 1 refers to resonance frequency at 4.1 GHz with a poor amplitude of −9.76 dB. This outcome means that the absorption does not reach 90% at any point on the selected spectrum. In Design 2, four curves connected with four triangles are added inside the resonator from Design 1 to consist of closed ring resonators (CRRs). The reflection coefficient of design 2 has a large bandwidth between 3.91 and 6 GHz above −10 dB value (absorptivity more than 90%). This increase in the absorption bandwidth is due to highly stored energy between the two rings. Design 3 involves inserting a cross-shaped patch between the triangles of the inner ring. The reflection coefficient of Design 3 increases absorption bandwidth to cover broadband between 4 and 7 GHz. This design increases absorption bandwidth because a second resonance frequency is observed at 6.37 GHz in addition to the first resonance frequency at 4.64 GHz. The superposition method of resonance frequencies can explain the expansion of absorption bandwidth. This technique combines different resonance peaks or modes that are dissimilar but have the same order [17]. The final design (proposed) is the same last design but with the addition four small slits on cross-shaped patch. These slits with dimensions S1×S2 improve the reflection coefficient at the beginning of the absorption bandwidth.

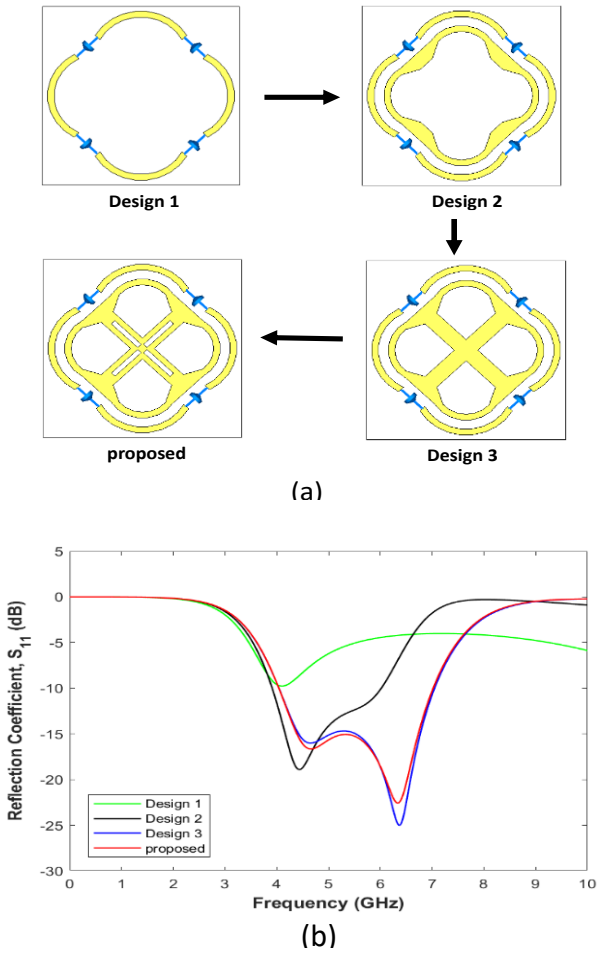


**Fig. 3. (a) Parametric analysis of the proposed structure and (b) Simulated reflection coefficient ($S_{11}$) in dB for various designs of the proposed structure**

## 4. Simulation Setup and Methodology

Numerical simulations were performed utilizing CST Studio Suite software, which involves 3D full-wave simulation. The periodic boundary conditions of the unit cell were applied in the X- and Y-axis directions to model the electric field and magnetic field of an infinite array, while open (add space) boundary was utilized in the +Z direction and the incident wave was applied along −Z by Floquet port for the TE and TM modes, as shown in Figure 4a. The unit cell was simulated in the transverse electromagnetic (TEM) mode by being placed between waveguides organized along the Z-axis in opposite directions. These waveguide ports were excited by an EM wave propagated along the Z-axis, as shown in Figure 4b. Boundary conditions were established along the X- and Y-axis directions

to achieve perfect electric field (PEC) and perfect magnetic field (PMC). These procedures guaranteed precise evaluation and inspection of the MM absorber properties and behavior. The tetrahedral meshing method was utilized to make a mesh and perform simulation between 0 and 10 GHz utilizing the frequency domain solver approach.

Accurate identification of MM absorption characteristics is important for achieving optimal RFEH. Absorption is critical for the efficiency of these structures in collecting EM radiation and converting it into electrical power. MM structures can be optimized by carefully evaluating their performance. This exacting modification calibrates MM to receive energy from particular frequency bands. Therefore, reliable measurements of MM absorption are very important for exploiting these structures in energy harvesting. The absorptivity of unit cell regarding frequency can be calculated by the equation below:

$$A(W) = 1 - |S_{11}(W)|^2 - |S_{21}(W)|^2 \quad \ldots(1)$$

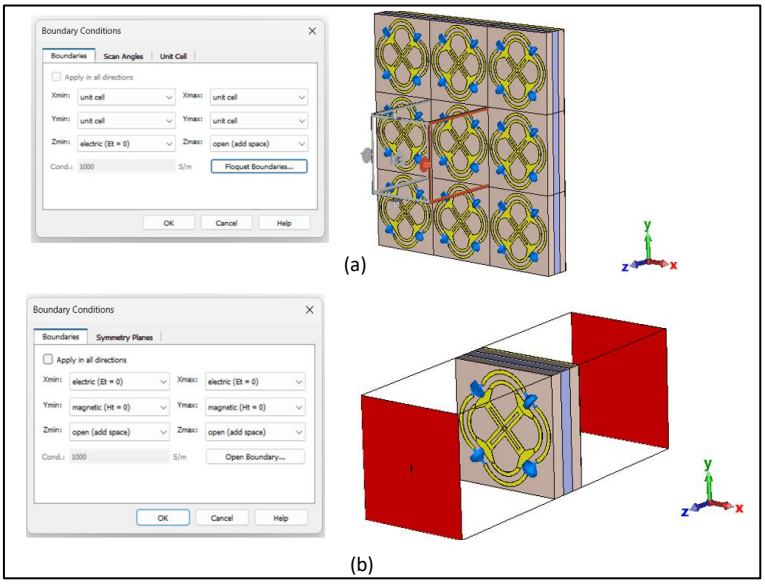


**Fig. 4. Boundary condition setup during the simulation of unit cell in CST: (a) TE and TM modes, (b) TEM mode**

where $|S_{11}(W)|$ refers to the absolute value of the overall reflection coefficient, and $|S_{21}(W)|$ indicates the absolute value of the overall transmission coefficient. The absorptivity can be optimized to reach the maximum value by modifying the unit cell structure to reduce the transmission and reflection parameters at the resonance frequency. The full ground plan on the bottom layer helps achieve high absorption efficiency by reducing the transmit power to a very small value that may be considered zero. After that, the absorptivity in Equation (1) written as follows:

$$A(W) = 1 - |S_{11}(W)|^2 \quad \ldots(2)$$

Complex scattering parameters (S-parameters) can be obtained according to a robust approach technique by the following equations [45]:

$$S^{11} = \frac{R^{01}\left(1 - e^{i2nk_0d}\right)}{1 - R^{012}e^{i2nk_0d}} \quad \ldots(3)$$

$$S^{21} = \frac{(1 - R^{012})e^{i2nk_0d}}{1 - R^{012}e^{i2nk_0d}} \quad \ldots(4)$$

where $R_{01} = \frac{z-1}{z+1}$. The impedance ($z$) of the MM unit cell can be calculated by using the following equation:

$$z = \pm\sqrt{\frac{(1 + S_{11})^2 - {S_{21}}^2}{(1 - S_{11})^2 - {S_{21}}^2}} \quad \ldots(5)$$

$$e^{ink_0d} = x \pm i\sqrt{1 - x^2} \quad \ldots(6)$$

$$x = \frac{1}{2S_{21}(1 - {S_{11}}^2 + {S_{21}}^2)} \quad \ldots(7)$$

where $d$ represents the prototype thickness, while $k_0$ represents to free space wave vector.

Impedance matching theory can explain the MM absorber mechanism. The MM unit cell effective impedance can be modified to align the free space

$$\ldots(8)$$

impedance by tuning the real and imaginary components of the permeability ($\mu$) and permittivity ($\varepsilon$). Antiparallel currents that generate between metal layers (resonator and ground plan) refer to permeability, which is responsible for magnetic resonance. The surface current generated on the top metal layer (resonator) of the MM structure refers to permittivity, which is responsible for electrical resonance. Consequently, the maximum absorption efficiency can occur at ( $z_{mm} = z_{free-space}$), and Equation (5) can be written as follows [31]:

$$z = \pm\sqrt{\frac{\mu}{\varepsilon}} \quad \ldots (8)$$

Figure 5 demonstrates the simulated reflection and absorption responses at normal incidence of the MM absorber. The frequency range of 6.09 to 6.52 GHz achieves a near-unity absorbance of nearly 99%. Moreover, a 90% broadband absorptivity is realized across the 4 to 7 GHz frequency range.

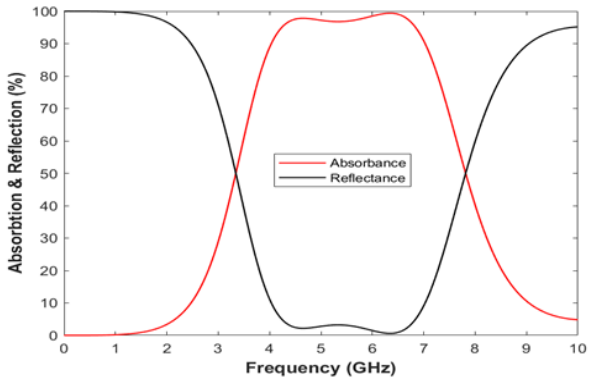


**Fig. 5. Simulated reflection and absorption efficiency of the proposed MM absorber under normal incidence**

MM absorbers should be analyzed as an array structure and contrasted with findings of the unit cell to enhance their EM behavior and achieve thorough understanding. In addition, array structure reflection and absorption coefficients can provide adequate knowledge about the ramification of coupling effect and interelement interactions. Figure 6(a) demonstrates the 3D model of the 3×3 array structure. Furthermore, the reflection and absorption values of this array structure were computed and compared with the unit cell results, as shown in Figure 6b. The results demonstrate a very minor alteration in the findings of the array structure and its unit cell. The slight difference in the correlation between the reflection and absorption values between a 3×3 array structure and an MM unit cell is mostly attributable to mutual coupling effects across adjacent cells. The effects of mutual coupling between the cells in the array can be neglected due to the small implications for the results. The behavior of the unit cell effectively reflects an array structure behavior, validating the robustness of the design in the array and single forms. Moreover, the strong correlation between the array structure and unit cell parameters in energy harvesting systems can achieve many benefits, such as improved bandwidth performance, impedance matching, enhanced efficiency, energy collection optimization, scalability, and flexibility. Furthermore, the identical absorption results for the array structure and unit cell in the figure below can guarantee reliable, efficient energy harvesting performance. Alignment of absorption properties between the two structures makes the array absorb incoming energy uniformly over its whole surface. The consistency of the array structure boosts energy harvesting by guaranteeing that each element contributes similarly in the harvesting operation.

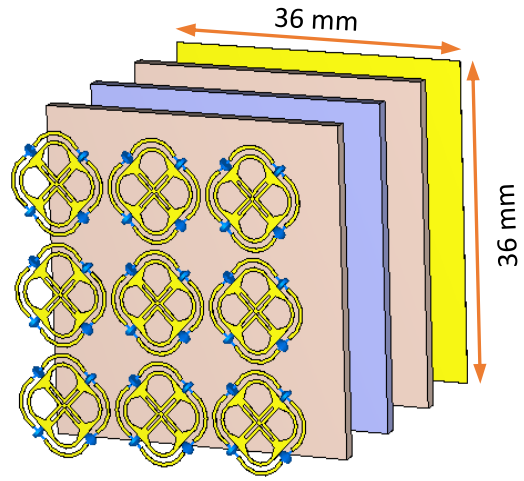


(a)

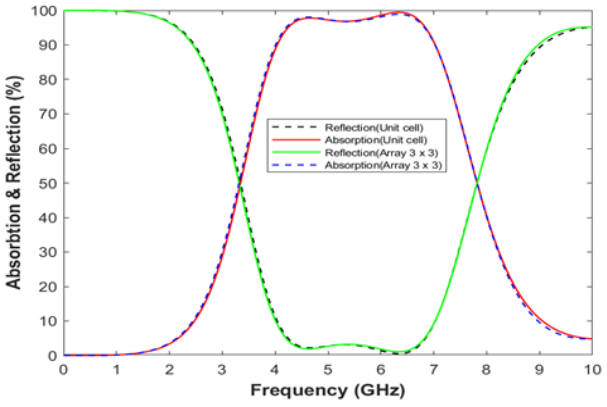


(b)

**Fig. 6. (a) 3D representation of a 3×3 array structure, (b) Simulated reflection and absorption efficiency of the unit cell and 3×3 array structure**

## 5. Parametric Study

Various factors performed a vital role in the proposed design to achieve maximum absorption efficiency, impedance matching, bandwidth expansion, and enhance the harvesting efficiency. First, the suitable dielectric substrate can improve the harvesting efficiency by delivering a large value of absorbed power from the resonator surface to the resistive loads instead of dissipating in a substrate. To discuss the effect of various substrate material types on design performance, three different materials were examined to identify the ideal substrate for the suggested design, considering the availability of materials and their costs. The materials included Rogers RO4350B (lossy), Rogers RO4003C (lossy), and FR-4 (lossy). The physical characteristics of these materials, particularly, dielectric constant ($\epsilon_r$) and loss tangent (tan δ), were verified. Rogers RO4350B substrate has a loss tangent of 0.0037 and a dielectric constant of 3.66. Rogers RO4003C substrate has a loss tangent of 0.0027 and a dielectric constant of 3.55. Last, FR-4 substrate has a loss tangent of 0.025 and a dielectric constant of 4.3. The thicknesses of all three substrates are the same (1.5 mm). The reflection coefficient was individually examined for the substrates, and the absorption efficiency was calculated by Equation (2). For instance, for Rogers RO4350B, the unit cell exhibits absorption above 90% between 4.2 and 7.4 GHz with a bandwidth of 3.2 GHz and maximum absorption efficiency of 99.86%. For Rogers RO4003C, the unit cell exhibits absorption above 90% between 4.24 and 7.58 GHz with bandwidth of 3.34 GH and maximum absorption efficiency of 99.88%. Last, for FR-4 substrate, the unit cell exhibits absorption above 90% between 4 and 7 GHz with bandwidth of 3 GHz and maximum absorption efficiency of 99.05%. These results are shown in Figure 7.

The value of maximum absorption efficiency for different substrates can indicate the effect of dielectric substrate losses (loss tangent value) on the design performance. Low-loss substrates can achieve perfect harvesting by transferring absorbed power to loads rather than dissipating in a substrate. The dielectric constant effect on the design performance is related to the following equations:

$$f = \frac{1}{2\pi\sqrt{LC}} \quad \ldots (9)$$

$$C = \varepsilon_0 \varepsilon_r \frac{A}{d} (F) \quad \ldots (10)$$

The dielectric constant ($\varepsilon_r$) is directly proportional to the equivalent capacitance ($C$), as shown in Equation (10). The resonance frequency ($f$) is inversely proportional to the equivalent capacitance according to Equation (9) [46]. As a result, the resonance frequency is different for each substrate material due to varied dielectric constant values. The MM unit cell resonance frequencies decrease for higher substrate dielectric constant ($\varepsilon_r$) values and increase for lower substrate dielectric constant ($\varepsilon_r$) values. This analysis closely matches the results in Figure 7. Although Rogers RO4003C substrate can achieve simple superiority in bandwidth and maximum absorption efficiency over FR-4 substrate, this slight superiority is offset by the availability and low costs of FR-4. Therefore, the substrate selected for the suggested design was FR-4.

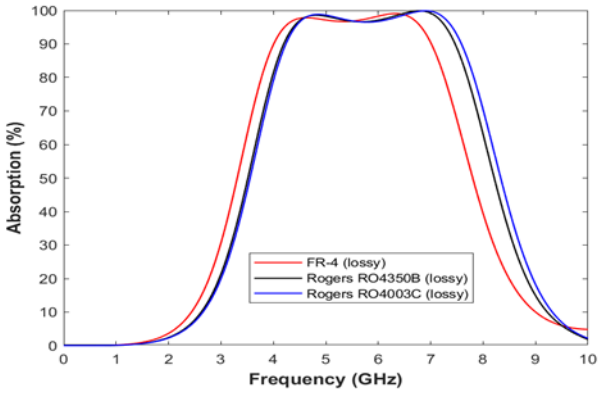


**Fig. 7. Simulated absorption efficiency for the various substrate materials**

To prove the validity of the FR-4 choice despite the high dielectric loss, Figure 8 demonstrates the absorption efficiency of two distinct substrate states. The findings display nearly identical absorption of the FR-4 substrate under loss-free and loss states.

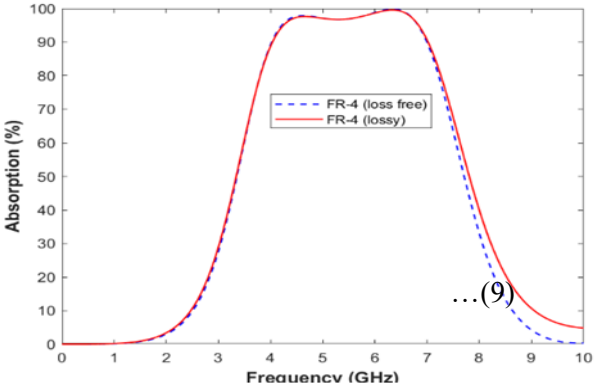


**Fig. 8. Simulated absorption efficiency under two different substrate states**

Air layer contributes to improving the absorption bandwidth, where it acts as an air cavity confined the waves inside the air layer. Figure 9 demonstrates the absorption efficiency of the MM unit cell with and without air layer.

Figure 10 exhibits the absorption efficiency as the thickness of the air layer is reduced from 6 mm to 1.5 mm in the step of 1.5 mm. When the air layer thickness decreases, the resonance frequency moves to the right, the absorption efficiency increases, and the absorption bandwidth larger than 90% is broadened. This resonance frequency shifts due to decreasing the effective permittivity when decreasing air layer thickness according to Equations (9) and (10). In general, the insertion of the air gap reduces the effective permittivity and improves the absorption bandwidth. The air layer thickness of 1.5 mm in the proposed design accomplishes an absorption efficiency of more than 90% throughout the frequency spectrum 4 to 7 GHz.

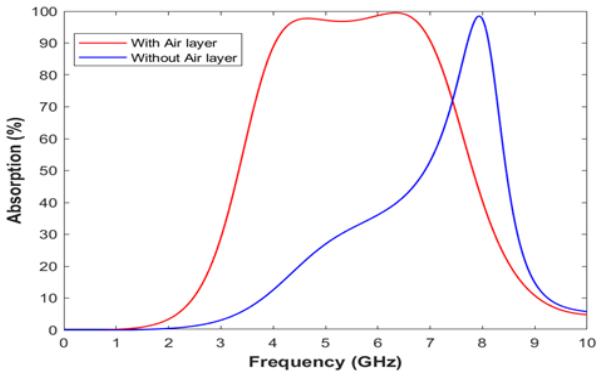


**Fig. 9. Simulated absorption efficiency of the unit cell with and without air layer**

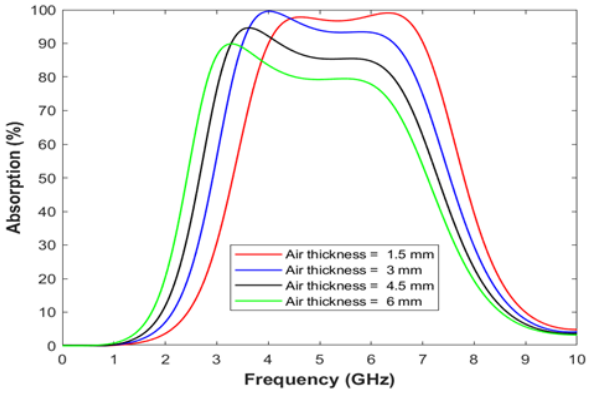


**Fig. 10. Simulated absorption efficiency for different air layer thicknesses**

Last, the value of resistances that serves as a lumped element between the resonator splits in the top layer was analyzed between 50 and 200 Ω with 50 Ω steps. Figure 11 shows the absorption bandwidth larger than 90% is perfect at 100 Ω and is reduced when the resistance value is increased; at 50 Ω resistance, two peaks at 4.1 and 6.88 GHZ with high decline between them are observed. Consequently, an optimal match between the MM unit cell impedance and free space impedance (377 Ω) can be attained by selecting the lumped resistance value of R = 100 Ω, an approach leading to ideal broadband absorption. To demonstrate the effects of resistors on the unit cell resonator, the absorption efficiency was compared with the scenario where no resistors are loaded on the unit cell resonator. The simulation results are shown in Figure 12. The maximum absorption efficiency is around 16.4% at a frequency range between 5.61 and 5.8 GHz without resistor loads. The decline in absorption is due to mismatch impedance between the unloaded resistor unit cell and free space, where the unit cell depends on lumped resistors to reduce the impedance value and match with free space impedance. Therefore, lumped resistors are essential for achieving maximum absorption efficiency and broad bandwidth.

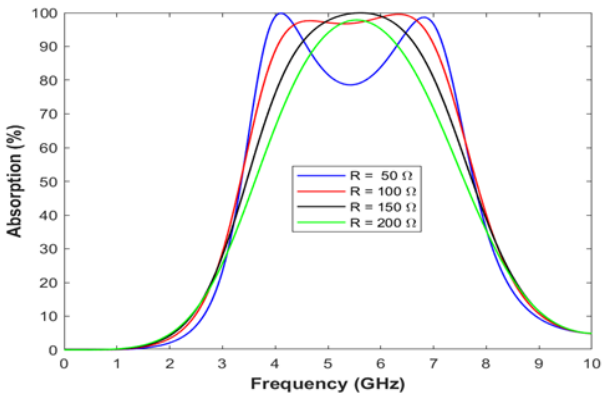


**Fig. 11. Simulated absorption efficiency for the different lumped resistors**

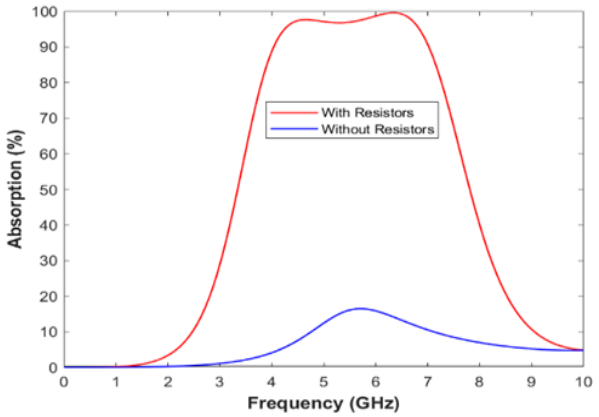


**Fig. 12. Simulated absorption efficiency of the unit cell with and without lumped resistors**

## 6. Electric Field (E-Field), Magnetic Field (H-Field), and Surface Current Distribution Analysis

The excitation of electric and magnetic fields is essential for MM absorber design. The electric field focused on the top layer resonator can be seen as a source of electric stimulation. The magnetic field can be activated by two currents moving in opposite directions through metal plates. The absorption efficiency can be increased to lead a maximum harvesting efficiency when magnetic and electric fields happen simultaneously.

To understand the physical behavior of absorbing and gathering EM radiation by the suggested MM design, magnetic field, electric field, and surface current distributions at 4.64 and 6.34 GHz were examined, as plotted in Figure 13. These frequencies were selected due to the highest absorption levels at these points. Figure 13a describes the surface current distribution at the frequencies of 4.64 and 6.34 GHz. At 4.64 GHz, the surface current distribution is concentrated on the outer curves because of the matches between the wavelength and outer resonator size. Current distribution at the upper and lower curves is dissipated to the right lumped resistors, and small current intensity in the left curve is directed to both left lumped resistors. However, at 6.34 GHz, the current intensity is concentrated in the outer and inner curves. The surface current distribution in the top metallic layer at both resonance frequencies is antiparallel; thus, the MM design has a substantial magnetic resonance. In addition, the matching impedance between the lumped resistors value and resonator makes the most absorbing energy directed from the top layer resonator to the lumped resistors, an outcome causing increased absorbing efficiency and achieving maximum energy harvesting.

Figure 13b illustrates the E-field distribution of the proposed design at frequencies of 4.64 and 6.34 GHz. Both figures utilize color gradients to demonstrate the electric field strength and distribution within the unit cell. Strong electric field intensity is shown in yellow and red zones, whereas low field intensity appears in green and blue. The E-field is concentrated in the left and right curves for inner and outer structures at 4.64 GHz. Th e E-field distribution is stronger in the outer left and right curves in addition to a small area on the sides of the outer upper and lower curves at 6.34 GHz. Figure 13c demonstrates the H-field distribution of the proposed unit cell at frequencies of 4.64 and 6.34 GHz. The H-field intensity is concentrated in the upper and lower curves for the inner and outer structures and in a small area on the sides of the left and right curves at both frequencies, with greater strength at 6.34 GHz. At each resonance frequency, the E-field and H-field exhibit almost inverse excitation patterns.

The introduced unit cell design comprises multiple subwavelength parts interacting with incoming EM waves at particular resonance frequencies. These parts are engineered to achieve resonance when the frequency of the incident wave matches their own, an outcome producing pronounced electric and magnetic reactions within the MM design. When resonance occurs, magnetic and electric fields are created within the MM structure by the incoming EM waves, and magnetic and electric oscillating dipole are produced. The dipoles establish concentrated magnetic and electric fields that are a powerful couple with the incoming EM waves, an outcome improving the total interaction. The coupling becomes more effective when the MM structure impedance matches the free space impedance at the resonance frequencies; this situation limits the reflection and increases the flow of energy into the MM structure.

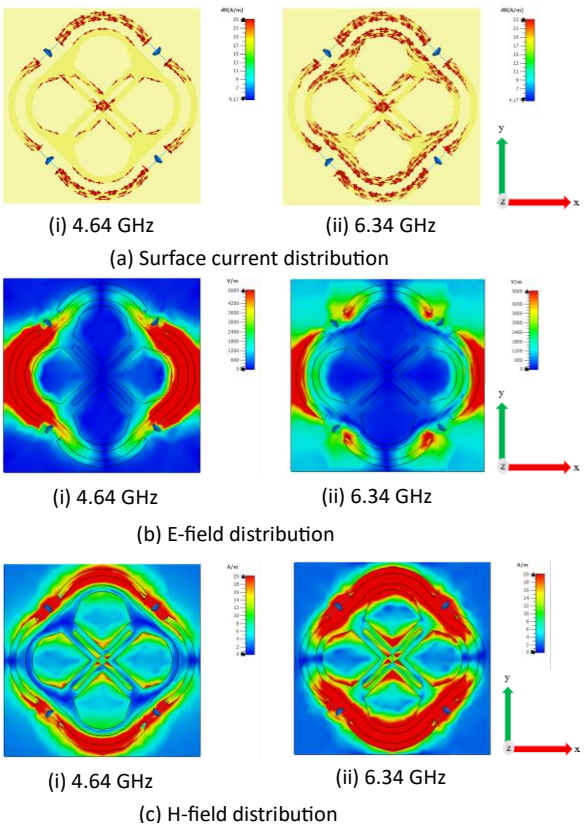


**Fig. 13. Simulation results of (a) surface current, (b) E-field, and (c) H-field distribution of the MM unit cell at (i) 4.64 GHz and (ii) 6.34 GHz**

## 7. Results and Discussion

### 7.1. Absorption Efficiency of the MM Unit Cell for Different Modes

The absorption efficiency of the proposed MM structure was calculated for the TE, TM, and TEM modes individually at the normal incident, as shown in Figure 14.

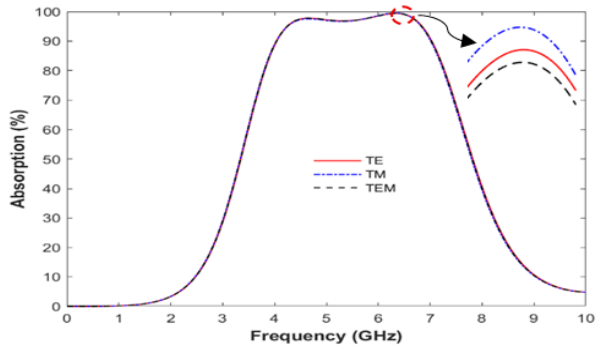


**Fig. 14. Simulated absorption efficiency of the MM unit cell for TE, TM, and TEM modes**

All modes present identical results of absorptivity regardless of the polarization mode because of the symmetrical configuration of the suggested MM structure. The broadband absorptivity larger than 90% is achieved between the 4 and 7 GHz frequency range for all modes.

### 7.2. Absorption Efficiency of the MM Unit Cell for Different Polarization and Incident Angles

The absorption efficiency of the proposed structure was carefully evaluated for various TE and TM angles to guarantee the MM design is optimal for a broad range of incident and polarization wave conditions. This approach improves their adaptability, reliability, and efficiency and make them suitable for practical application.

Figures 15 and 16 illustrate the absorption efficiency for different polarization angles in the TE and TM modes, respectively. Polarization angle ($\phi$) sweeping from 0° to 90° with a step of 15° and the incident angle is kept unchanged at 0°. In the TE mode, the E-field is stationary and perpendicular to the path of wave traveling while the H-field and wave traveling vector revolves by an angle (θ). In the TM mode, the H-field is stationary and perpendicular to the path of wave traveling while the E-field and wave traveling vector revolve by an angle (θ). Figures 15 and 16 reveal that the incident waves with different polarization angles exhibit the same absorption response for the TE and TM modes due to the favorable geometric symmetry of MM structure. This extreme symmetry of the proposed design makes it polarization insensitive, where absorbed energy by electric and magnetic resonance in the MM structure remains identical for incoming waves with different polarization angles. Consequently, the proposed MM absorber can deal with the horizontal, vertical, and circular polarization waves.

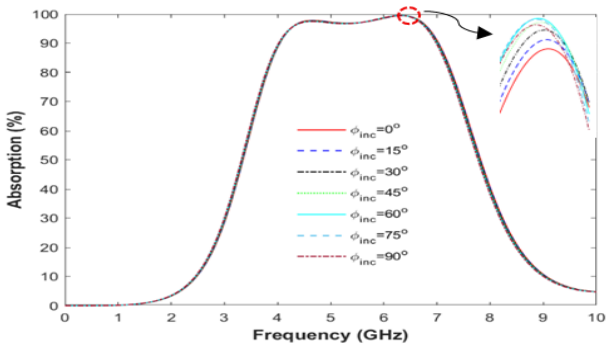


**Fig. 15. Simulated absorption efficiency of the MM unit cell for various polarization angles (TE)**

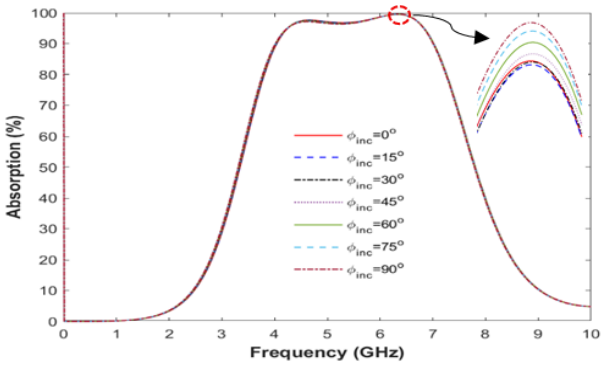


**Fig. 16. Simulated absorption efficiency of the MM unit cell for various polarization angles (TM)**

The numerical findings indicate that this design is suitable for EM energy harvesting because the achieved perfect absorption is insensitive to wave modes and polarization angle.

In the real-world scenario, the EM wave's direction is unknown and almost incident at an angle with respect to the MM structure. Therefore, designing an MM absorber that can gather ambient EM energy with wide incident angles is recommended. The reflection coefficient for the oblique incident in TE and TM polarization can be expressed as follows:

$$\Gamma_{TE} = \frac{Z(w)\cos\theta_i - Z_0\cos\theta_t}{Z(w)\cos\theta_i + Z_0\cos\theta_t} \quad \ldots(11)$$

$$\Gamma_{TM} = \frac{Z(w)\cos\theta_t - Z_0\cos\theta_i}{Z(w)\cos\theta_t + Z_0\cos\theta_i} \quad \ldots(12)$$

where $\theta_i$ and $\theta_t$ represent the incident angle and transmission angle, respectively; $Z_0$ and $Z(w)$ represent the free space impedance and MM resonator impedance, respectively. Based on the equations above, when the incident angle ($\theta_i$) varies, so does the reflection coefficient ($\Gamma$). The proposed MM absorber was examined to evaluate its capacity for capturing incident waves from different incident angles for TE and TM polarization, as shown in Figures 17 and 18, respectively. The incident angle ($\theta_i$) changes from 0° to 60° in step of 15°, and the polarization angle ($\phi$) is kept fixed at 0°. Figure 17 exhibits that the absorption bandwidth for TE polarization stays constant between 0° and 15°, and absorption efficiency is more than 90% between 4 and 7 GHz. When the angle of incident is increased from 15° to 30°, the absorption efficiency is slightly reduced with a small shift in resonance frequencies to the right side with absorption ratio more than 90% between 4.2 and 7.06 GHz, while absorption ratio at 4 GHz declines to 83.8%. At 45°, the absorption bandwidth more than 90% is reduced to achieve a ratio between 5,64 and 7.1 GHz, while absorption efficiency starts from 75.6% at 4 GHz and reaches 93.4% at 7 GHz with maximum efficiency of 98.5% at 6.65 GHz. Additionally, when the angle varies to 60°, the absorption bandwidth more than 90% is reduced to achieve ratio between 6.38 and 7.05 GHz, while absorption efficiency starts from 61.1% at 4 GHz and reaches 91.8% at 7 GHz with maximum efficiency of 94.85% at 6.78 GHz. In general, when the incident angle increases, the absorption efficiency decreases, but the absorption efficiency surpasses 61.1% up to incidence angle of 60° at frequency band between 4 and 7 GHz. The absorption efficiency decreases due to the MM absorber's improved ability to achieve electrical resonance in reaction to incident EM waves, as opposed to its more difficult magnetic resonance. With increased in incident angle in TE polarization, the component of magnetic field in the y-direction progressively reduces and results in a drop in magnetic flux. This leads to a misalignment of electrical and magnetic resonances, a mismatch impedance in the MM unit cell, and complicates the maintenance of high absorption rates.

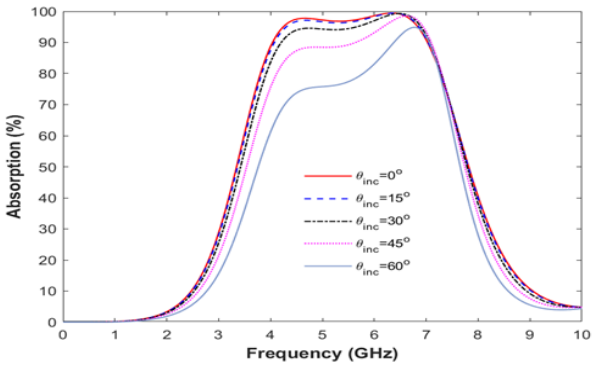


**Fig. 17. Simulated absorption efficiency of the MM unit cell for various incident angles (TE)**

For TM polarized incidence angles, as shown in Figure 18, the absorption efficiency stays constant up to 15°. When the angle of incidence rises from 15° to 30°, the absorption efficiency is slightly reduced with a small shift in resonance frequencies to the right side with absorption ratio more than 90% between 4.36 and 7.1 GHz, while absorption ratio at 4 GHz declines to 78%. At this angle, the absorption response is identical to the previous incident angles over the band between 5.05 and 6.65 GHz. At 45°, the absorption bandwidth more than 90% is reduced to achieve a ratio between 4.82 and 7.12 GHz, while absorption efficiency is 65% at 4 GHz and maximum efficiency of 96.5% at 6.5 GHz. When the angle varies to 60°, the absorption efficiency does not reach 90% and the maximum absorption efficiency is 87.3% at 5.98 GHz. Overall, the magnetic field stays continuously aligned in the y-direction in the TM mode. This alignment guarantees a consistent response to the magnetic field and results in a powerful magnetic resonance and significant amounts of absorptivity at various angles.

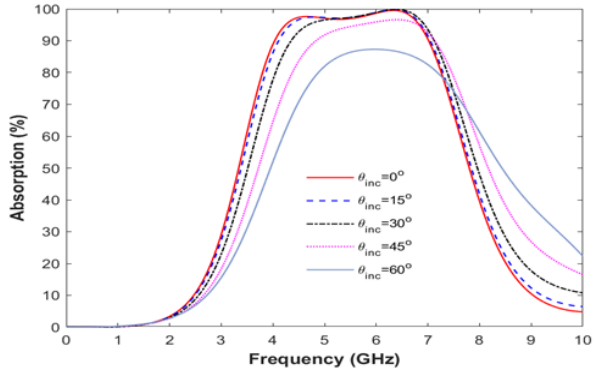


**Fig. 18. Simulated absorption efficiency of the MM unit cell for various incident angles (TM)**

### 7.3. Analysis of the Proposed Structure's Harvesting Efficiency

Energy harvesting functionalities of the proposed design were examined by loss balance analysis. A thorough 3D full-wave simulation by CST studio suite was performed to examine the distribution of dissipated power within the unit cell. Floquet port was used to excite the proposed unit cell along the Z-axis with incident power tuned at 0.5 watt. This method enabled computing the dissipated power in the resistive loads, metal cover, dielectric substrate, and resonator. Figure 19 displays power delivered to the unit cell. The unit cell's accepted power is more than 0.45 watt across the desired band, which is equivalent to 90% of the incident power (0.5 watt). The accepted power is represented by the absorbed power in the unit cell. Furthermore, the power dissipated in resistor loads is more than 0.4 watt during the operating frequency, which is equivalent to 80% of the incident power. Power loss in dielectric substrate ranges between 5.4% and 9.6% at the operating frequency and. Last, the value of power loss in copper is very small and negligible. The high loss tangent value of the FR-4 substrate contributes to high power loss on the substrates. These losses can be avoided by using other substrates with low loss tangent values, as mentioned in Figure 7, or by adding lumped elements in particular places on the resonator to dissipate the absorption power through it. Moreover, the high value of power dissipation in the resistor loads can be related to reasons including the efficient impedance alignment between the MM unit cell and free space and the suitable selection of the values and places of resistor loads.

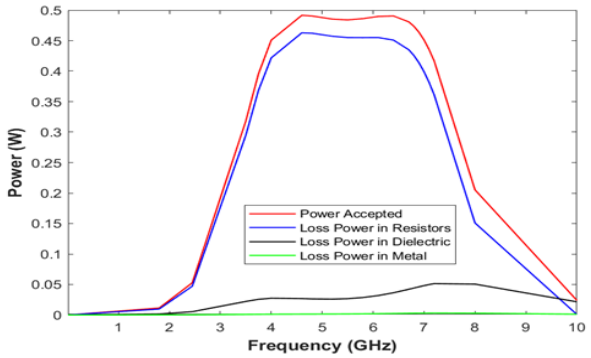


**Fig. 19. Power distribution in MM unit cell structure**

The energy harvesting efficiency (RF to AC power converting efficiency) of the MM unit cell was calculated using the following formula [12]:

$$harvesting\ efficiency(\%) = \frac{P_{load}}{P_{incident}} \times 100 \quad \ldots(13)$$

where $P_{load}$ denotes the total power dissipated in the resistor loads, and $P_{incident}$ is the total incident power on the MM structure. The harvesting efficiency of the unit cell was evaluated for different polarization ($\phi$) and incident angles (θ) in the TE and TM modes to ensure the effective of MM structure in practical environment, where incident EM waves have unknown polarization and direction. Figures 20 and 21 illustrate the harvesting efficiency for different polarization angles in the TE and TM modes, respectively. Polarization angle ($\phi$) varies from 0° to 90° with a step of 15°, and the incident angle is kept unchanged at 0°.

Figure 20 shows the harvesting efficiency of the unit cell in TE mode at different polarization angles is above of 80% over the desired resonance band and more than 90% across the range between 4.28 and 6.48 GHz with maximum efficiency of 92.24% at 4.6 GHz. The results in the TM mode are identical with those in the TE mode, as shown in Figure 21.

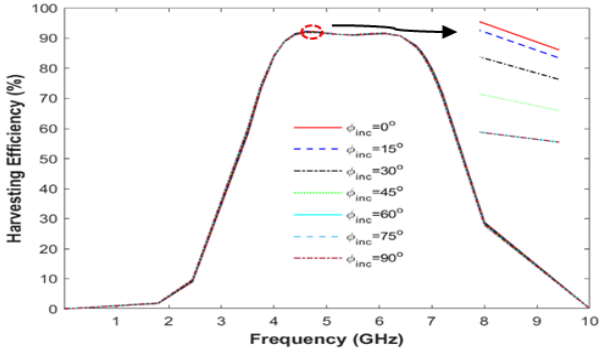


**Fig. 20. Simulated harvesting efficiency of the MM unit cell for various polarization angles (TE)**

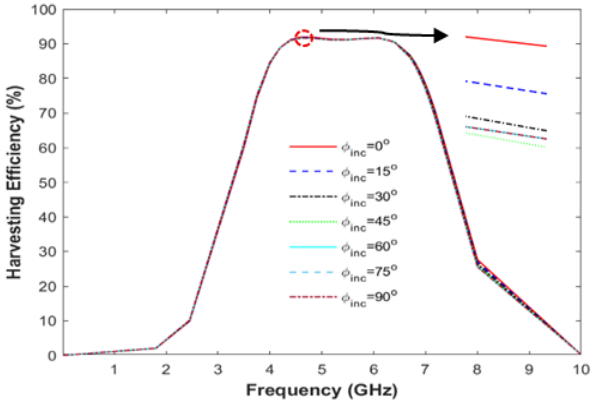


**Fig. 21. Simulated harvesting efficiency of the MM unit cell for various polarization angles (TM)**

...(13)

Finally, the harvesting efficiency of the unit cell remains unaffected by polarization because resistors share the cell's power equally when the polarization angle changes from 0° to 90°. The amount of delivered power to each resistor is different for various polarization angles, but the sum of the resistors' contributions is equal.

Furthermore, CST studio was used to examine the proposed structures' harvesting efficiency numerically under different incident angles ($\theta_i$) for the TE and TM modes, as shown in Figures 22 and 23, respectively. The incident angle ($\theta_i$) changes from 0° to 60° in steps of 15°, and the polarization angle ($\phi$) is kept fixed at 0°. Figure 22 illustrates the harvesting efficiency of the unit cell in TE mode at $\theta_i$= 0° is above 80% over the desired resonance band and more than 90% across the range between 4.44 and 6.47 GHz with maximum harvesting efficiency of 92.15% at 4.6 GHz. When the incident angle $\theta_i$= 15°, the results are identical to the previous normal incidence with maximum harvesting efficiency of 91.51% at 4.6 GHz. When the angle of incident increases from 15° to 30°, the harvesting efficiency is slightly reduced with a ratio above 80% over the desired resonance band, and maximum harvesting efficiency is 90.32% at 6.4 GHz. For angle $\theta_i$ = 45°, the harvesting efficiency starts from 72% at 4 GHz and reaches 80.2% at 7 GHz with maximum value of 88.34% at 6.4 GHz. The substantial decrease in harvesting efficiency occurs at the angle $\theta_i$ = 60° with achieved peak value of 83% at 6.7 GHz. In TM polarized incidence angles, as shown in Figure 23, the harvesting efficiency stays above 80% over the desired resonance band and more than 90% across the range between 4.29 and 6.44 GHz with maximum harvesting efficiency of 91.93% at 4.6 GHz. When the incident angle $\theta_i$ = 15°, the results are the same as the preceding normal incidence with maximum harvesting efficiency of 91.96% at 6.1 GHz. When the angle of incident rises from 15° to 30°, harvesting efficiency decreases marginally with a maximum harvesting efficiency of 92.12% at 6.1 GHz and a ratio above 80% over the targeted resonance band. At angle $\theta_i$ = 45°, the harvesting efficiency started from 62% at 4 GHz and reaches 81% at 7 GHz with maximum value of 89.45% at 6.1 GHz. For angle $\theta_i$ = 60°, harvesting efficiency considerably decreases and achieves a peak value of 81.42% at 5.8 GHz.

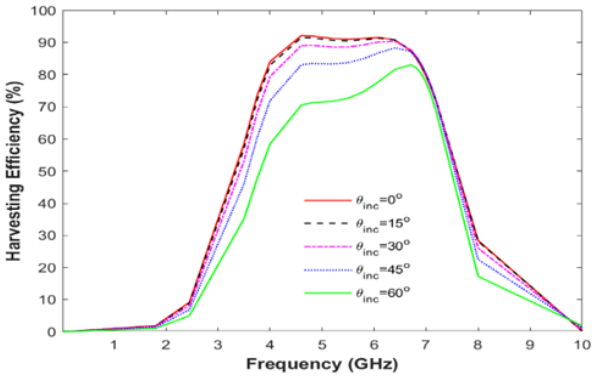


**Fig. 22. Simulated harvesting efficiency of the MM unit cell for various incidence angles (TE)**

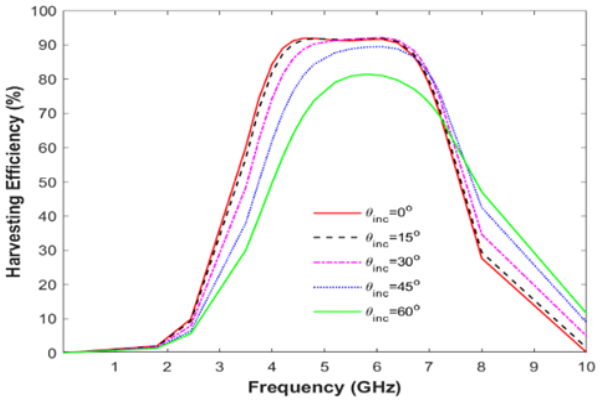


**Fig. 23. Simulated harvesting efficiency of the MM unit cell for various incidence angles (TM)**

The proposed structure displays high efficiency at normal incidence, an outcome demonstrating its exceptional performance in typical conditions. Additionally, the results show a consistent level of ideal performance even when the incident angle is increased to 30°. However, harvesting efficiency drops when the angle of incident reaches 60°. This finding highlights the importance of considering the incident angle when attempting to improve the efficiency of power transfer and suggests a possible disadvantage in the structures' performance when employed at greater incidence angles.

Resistive loads (lumped elements) are a critical component in an energy harvester's construction. The ideal resistance value for our suggested structure is ascertained by positioning different resistive loads within the resonator gaps. The harvesting efficiency is evaluated for different load values starting from 50 Ω and reaching 200 Ω with a step of 50 Ω, as shown in Figure 24.

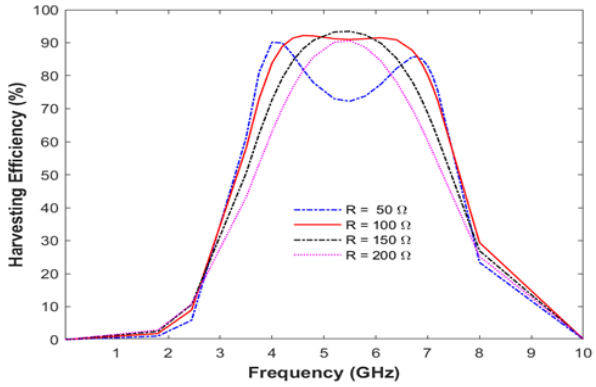


**Fig. 24. Simulated harvesting efficiency for the different resistive loads**

When the resistive load value is 50 Ω, the harvesting efficiency remains below 80% over the large band between 4.7 and 6.25 GHz and has a maximum value of 90.14% at 4 GHz. The largest bandwidth of good harvesting performance is achieved when using a 100 Ω resistor load. In addition, the bandwidth of harvesting efficiency above 80% is reduced at 150 and 200 Ω.

Table 2 compares the suggested MM design with other published work findings in terms of the absorption bandwidth, overall size, polarization insensitivity, and angular stability at oblique incidence. The introduced design offers a large bandwidth in a more compact size. Furthermore, the MM design has a small total thickness of 4.57 mm or 0.06 times the wavelength that corresponds to the lowest operating frequency. Moreover, the proposed design is independent of the polarization states of incident waves, so it is suitable in the field of EM energy harvesting to power the WSNs and low-power electronic devices.

**Table 2,**
**Comparison with previous works**

| Ref. Year | 90% Absorption Bandwidth (GHz) | Absorption | Relative absorption bandwidth | Unit cell size (mm³) | Polarization insensitive (TE and TM modes ?) | Angular stability | Dielectric material |
|---|---|---|---|---|---|---|---|
| [15] | 12.3–14.8 | >90% | 18.45% | 18.7×18.7×3.27 (0.766×0.766×0.134) $\lambda_0$ | Both | 0–45° | FR4 |
| [39] | 1.94–2.98 | >90% | 42.6% | 55.7×55.7×18.27 (0.46×0.46×0.152) $\lambda_0$ | Both | 0–45° | FR4 |
| [42] | 7.8–12.6 | >90% | 47% | 16.6×16.6×3.27 (0.565×0.565×0.11) $\lambda_0$ | NA | 0–30° | FR4 |
| [43] | 1.89–6.85 | >90% | 113% | 40×40×17.27 (0.25×0.25×0.108) $\lambda_0$ | Both | 0–45° | FR4 |
| [44] | 6.7–8.25 | >99% | 23.13% | 14×14×3.245 (0.312×0.312×0.072) $\lambda_0$ | Polarization sensitive | NA | Rogers/RT Duriod 5880 |
| This work | 4–7 | >90% | 75% | 12×12×4.57 (0.16×0.16×0.06) $\lambda_0$ | Both | 0–45° | FR4 |

## 8. Conclusion

This study presents a novel design of a compact, polarization-insensitive, wide-angle, and highly efficient MM structure. The proposed MM structure contains four lumped resistors within the resonator gaps to absorb a broad frequency range effectively. CST Studio Suite software is utilized in performing a thorough numerical evaluation. According to the numerical results, the proposed MM structure has a broadband absorption bandwidth of more than 90% in the 4 to 7 GHz frequency range, with a fractional bandwidth of 75%. The analysis of E-field, H-field, and surface current distributions is discussed to provide a deep understanding of the broad absorption mechanism. In addition, the MM unit cell remains insensitive to polarization at normal and oblique incident waves and exhibits broadband absorption at an angle of incident up to 45° for TE and TM polarizations. Accurate impedance matching between the MM structure and free space facilitates effective absorption and channeling of EM radiation power to the resistive loads and produce substantially higher harvesting efficiency above 80% within the targeted band. The promising power-harvesting capabilities and compact size of the introduced MM absorber make it the perfect choice for energy harvesting systems in WSNs and indicate major developments in technologies for WC and renewable energy usage. The broadband and polarization-independent features of this design enable efficient energy collection from multiple

sources and render it an optimal selection for extending the lifespan of WSNs and low-power electronic devices by using ambient EM radiation energy; this design reduces reliance on traditional power sources and promotes sustainable technologies.

## Conflict of interest

The authors declare that they have no conflict of interest.

## References

[1] X. Tang, X. Wang, R. Cattley, F. Gu, and A. D. Ball, "Energy harvesting technologies for achieving self-powered wireless sensor networks in machine condition monitoring: A review," *Sensors*, vol. 18, no. 12, p. 4113, 2018.

[2] S. Kawar, S. Krishnan, and K. Abugharbieh, "An Input Power-Aware Efficiency Tracking Technique with Discontinuous Charging for Energy Harvesting Applications," *IEEE Access*, vol. 8, pp. 135195–135207, 2020.

[3] O. Kanoun *et al.*, "Prospects of wireless energy-aware sensors for smart factories in the industry 4.0 era," *Electronics*, vol. 10, no. 23, p. 2929, 2021.

[4] A. J. Williams, M. F. Torquato, I. M. Cameron, A. A. Fahmy, and J. Sienz, "Survey of energy harvesting technologies for wireless sensor networks," *IEEE Access*, vol. 9, pp. 77493–77510, 2021.

[5] Y. C. Lee *et al.*, "High-performance multiband ambient RF energy harvesting front-end system for sustainable IoT applications—A review," *IEEE Access*, vol. 11, pp. 11143–11164, 2023.

[6] M. Wagih, A. S. Weddell, and S. Beeby, "Millimeter-wave power harvesting: A review," *IEEE Open J. Antennas Propag.*, vol. 1, pp. 560–578, 2020.

[7] E. D. Nwalike, K. A. Ibrahim, F. Crawley, Q. Qin, P. Luk, and Z. Luo, "Harnessing energy for wearables: a review of radio frequency energy harvesting technologies," *Energies*, vol. 16, no. 15, p. 5711, 2023.

[8] N. U. Khan, F. U. Khan, M. Farina, and A. Merla, "RF energy harvesters for wireless sensors, state of the art, future prospects and challenges: a review," *Phys. Eng. Sci. Med.*, vol. 47, no. 2, pp. 385–401, 2024.

[9] X. Zhang, H. Liu, and L. Li, "Electromagnetic power harvester using wide-angle and polarization-insensitive metasurfaces," *Appl. Sci.*, vol. 8, no. 4, p. 497, 2018.

[10] M. M. Hasan and A. M. A. Sabaawi, "Microstrip patch antenna with multi-fins for radio frequency energy harvesting applications," *Prog. Electromagn. Res. C*, vol. 142, pp. 61–73, 2024.

[11] S. Roy, J.-J. Tiang, M. Bin Roslee, M. T. Ahmed, A. Z. Kouzani, and M. A. P. Mahmud, "Design of a highly efficient wideband multi-frequency ambient RF energy harvester," *Sensors*, vol. 22, no. 2, p. 424, 2022.

[12] S. Costanzo and F. Venneri, "Polarization-insensitive fractal metamaterial surface for energy harvesting in IoT applications," *Electronics*, vol. 9, no. 6, p. 959, 2020.

[13] A. A. G. Amer, S. Z. Sapuan, and A. Y. I. Ashyap, "Efficient metasurface for electromagnetic energy harvesting with high capture efficiency and a wide range of incident angles," *J. Electromagn. Waves Appl.*, vol. 37, no. 2, pp. 245–256, 2023.

[14] A. A. G. Amer, S. Z. Sapuan, N. Nasimuddin, A. Alphones, and N. B. Zinal, "A comprehensive review of metasurface structures suitable for RF energy harvesting," *IEEE Access*, vol. 8, pp. 76433–76452, 2020.

[15] T. S. Pham, B. X. Khuyen, V. D. Lam, L. Chen, and Y. Lee, "Wide-Angle, Polarization-Independent Broadband Metamaterial Absorber by Using Plasmonic Metasurface-Based Split-Circular Structure," in *Photonics*, MDPI, 2025, p. 334.

[16] N. I. Landy, S. Sajuyigbe, J. J. Mock, D. R. Smith, and W. J. Padilla, "Phys. Rev. Lett. 100, 207402 (2008) - Perfect Metamaterial Absorber," *Phys. Rev. Lett.*, 2008.

[17] H. Zheng, T. S. Pham, L. Chen, and Y. Lee, "Metamaterial Perfect Absorbers for Controlling Bandwidth: Single-Peak/Multiple-Peaks/Tailored-Band/Broadband," *Crystals*, vol. 14, no. 1, p. 19, 2023.

[18] T. Lang, M. Xiao, and W. Cen, "Graphene-based metamaterial sensor for pesticide trace detection," *Biosensors*, vol. 13, no. 5, p. 560, 2023.

[19] A. S. Saadeldin, A. M. Sayed, A. M. Amr, M. O. Sayed, M. F. O. Hameed, and S. S. A. Obayya, "Wideband ultrathin and polarization insensitive metamaterial absorber for Ku-band applications," *J. Mater. Sci. Mater. Electron.*, vol. 34, no. 26, p. 1797, 2023.

[20] Y. Wei *et al.*, "A dual-band, polarization-insensitive, wide-angle metasurface array for electromagnetic energy harvesting and wireless power transfer," *Results Phys.*, vol. 46, p. 106261, 2023.

[21] A. M. Tamim, M. R. I. Faruque, M. J. Alam, S. S. Islam, and M. T. Islam, "Split ring resonator loaded horizontally inverse double L-shaped metamaterial for C-, X-and Ku-Band Microwave applications," *Results Phys.*, vol. 12, pp. 2112–2122, 2019.

[22] N. Ullah *et al.*, "A compact complementary split ring resonator (CSRR) based perfect metamaterial absorber for energy harvesting applications," *Eng. Sci. Technol. an Int. J.*, vol. 45, p. 101473, 2023.

[23] B. Ghaderi, V. Nayyeri, M. Soleimani, and O. M. Ramahi, "A novel symmetric ELC resonator for polarization-independent and highly efficient electromagnetic energy harvesting," in *2017 IEEE MTT-S International Microwave Workshop Series on Advanced Materials and Processes for RF and THz Applications (IMWS-AMP)*, IEEE, 2017, pp. 1–3.

[24] A. A. G. Amer *et al.*, "Dual-band, wide-angle, and high-capture efficiency metasurface for electromagnetic energy harvesting," *Nanomaterials*, vol. 13, no. 13, p. 2015, 2023.

[25] A. A. G. Amer, N. Othman, S. Z. Sapuan, A. Alphones, and A. A. Salem, "High-efficiency electromagnetic energy harvesting using double-elliptical metasurface resonators," *PLoS One*, vol. 18, no. 12, p. e0291354, 2023.

[26] A. Ghaneizadeh, K. Mafinezhad, and M. Joodaki, "Design and fabrication of a 2D-isotropic flexible ultra-thin metasurface for ambient electromagnetic energy harvesting," *Aip Adv.*, vol. 9, no. 2, 2019, doi: 10.1063/1.5083876.

[27] N. Ullah *et al.*, "Design and experimental validation of a compact dual-band metamaterial perfect absorber for electromagnetic energy harvesting applications," *Opt. Mater. (Amst).*, vol. 157, 2024, doi: 10.1016/j.optmat.2024.116054.

[28] N. Ullah *et al.*, "Design and experimental validation of a compact dual band double negative metamaterial for energy harvesting applications," *Sci. Rep.*, vol. 15, no. 1, 2025, doi: 10.1038/s41598-025-99298-w.

[29] S. D. Assimonis, T. Samaras, J. N. Sahalos, T. Kollatou, D. Tsiamitros, and D. Stimoniaris, "High efficiency and triple-band metamaterial electromagnetic energy hervester," in *Eleco 2015 9th International Conference on Electrical and Electronics Engineering*, 2016, pp. 320–323. doi: 10.1109/ELECO.2015.7394527.

[30] N. Ullah, M. S. Islam, A. Hoque, A. Alzamil, M. S. Soliman, and M. T. Islam, "Design and development of a compact, wide-angle metamaterial electromagnetic energy harvester with multiband functionality and polarization-insensitive features," *Sci. Rep.*, vol. 14, no. 1, 2024, doi: 10.1038/s41598-024-69976-2.

[31] M. Amiri, F. Tofigh, N. Shariati, J. Lipman, and M. Abolhasan, "Miniature tri-wideband Sierpinski-Minkowski fractals metamaterial perfect absorber," *Iet Microwaves Antennas Propag.*, vol. 13, no. 7, pp. 991–996, 2019, doi: 10.1049/iet-map.2018.5837.

[32] M. Norouzi *et al.*, "3D metamaterial ultra-wideband absorber for curved surface," *Sci. Rep.*, vol. 13, no. 1, 2023, doi: 10.1038/s41598-023-28021-4.

[33] B. Ghaderi, M. Soleimani, V. Nayyeri, and O. M. Ramahi, "Pixelated Metasurface for Dual-Band and Multi-Polarization Electromagnetic Energy Harvesting," *Sci. Rep.*, vol. 8, no. 1, 2018, doi: 10.1038/s41598-018-31661-6.

[34] A. Ghaneizadeh, M. Joodaki, J. Börcsök, A. Golmakani, and K. Mafinezhad, "Analysis, design, and implementation of a new extremely ultrathin 2-D-isotropic flexible energy harvester using symmetric patch FSS," *IEEE Trans. Microw. Theory Tech.*, vol. 68, no. 6, pp. 2108–2115, 2020.

[35] F. O. Alkurt *et al.*, "Octagonal shaped metamaterial absorber based energy harvester," *Medziagotyra*, vol. 24, no. 3, pp. 253–259, 2018, doi: 10.5755/j01.ms.24.3.18625.

[36] F. Yu, X. Yang, H. Zhong, C. Chu, and S. Gao, "Polarization-insensitive wide-angle-reception metasurface with simplified structure for harvesting electromagnetic energy," *Appl. Phys. Lett.*, vol. 113, no. 12, 2018.

[37] N. Ullah *et al.*, "An efficient, compact, wide-angle, wide-band, and polarization-insensitive metamaterial electromagnetic energy harvester," *Alexandria Eng. J.*, vol. 82, pp. 377–388, 2023.

[38] Y. I. Abdulkarim *et al.*, "A review on metamaterial absorbers: Microwave to optical," *Front. Phys.*, vol. 10, p. 893791, 2022.

[39] A. A. G. Amer, S. Z. Sapuan, N. B. Othman, A. A. Salem, A. J. A. Al-Gburi, and Z. Zakaria, "A wide-angle, polarization-insensitive, wideband metamaterial absorber with lumped resistor loading for ISM band applications," *IEEE Access*, vol. 12, pp. 42629–42641, 2023.

[40] C. Liang *et al.*, "A broadband perfect metamaterial absorber with angle-insensitive characteristics," *J. Electromagn. Waves Appl.*, vol. 37, no. 3, pp. 401–410, 2023.

[41] X. You *et al.*, "Ultra-wideband far-infrared absorber based on anisotropically etched doped silicon," *Opt. Lett.*, vol. 45, no. 5, pp. 1196–1199, 2020.

[42] T. Q. H. Nguyen, T. K. T. Nguyen, T. N. Cao, H. Nguyen, and L. G. Bach, "Numerical study of a broadband metamaterial absorber using a single split circle ring and lumped resistors for X-band applications," *AIP Adv.*, vol. 10, no. 3, 2020.

[43] A. A. G. Amer, S. Z. Sapuan, A. Alzahrani, N. Nasimuddin, A. A. Salem, and S. S. M. Ghoneim, "Design and analysis of polarization-independent, wide-angle, broadband metasurface absorber using resistor-loaded split-ring resonators," *Electronics*, vol. 11, no. 13, p. 1986, 2022.

[44] H. Ojukwu, B. Seet, and S. U. Rehman, "Wideband and load-insensitive metasurface absorber for radio frequency energy harvesting," in *2022 IEEE 33rd Annual International Symposium on Personal, Indoor and Mobile Radio Communications (PIMRC)*, IEEE, 2022, pp. 963–967.

[45] X. Chen, T. M. Grzegorczyk, B.-I. Wu, J. Pacheco Jr, and J. A. Kong, "Robust method to retrieve the constitutive effective parameters of metamaterials," *Phys. Rev. E—Statistical, Nonlinear, Soft Matter Phys.*, vol. 70, no. 1, p. 16608, 2004.

[46] M. R. Islam *et al.*, "Metamaterial based on an inverse double V loaded complementary square split ring resonator for radar and Wi-Fi applications," *Sci. Rep.*, vol. 11, no. 1, p. 21782, 2021

# تصميم ممتص مدمج عريض النطاق من مادة فوقية مع استقبال واسع الزاوية وغير حساس للاستقطاب لحصاد الطاقة الكهرومغناطيسية في تطبيقات شبكات الاستشعار اللاسلكي

**زين العابدين خالد فليح [١]*، يحيى علي لفتة [٢]**

[١،٢] قسم الهندسة الالكترونية والاتصالات، كلية الهندسة، جامعة الكوفة، النجف، العراق

*البريد الالكتروني : zainalabdink.alchallaby@student.uokufa.edu.iq

**المستخلص**

يقدم هذا العمل تصميمًا جديدًا لممتصّ عريض النطاق مدمج من مادة فوقية (MM)، يتميز باستقبال واسع الزاوية وغير حساس للاستقطاب، وذلك لتطبيقات حصاد الطاقة الكهرومغناطيسية المحيطة. تتكون خلية وحدة MM المقترحة من طبقتين من ركيزة FR-4 منخفضة التكلفة. تحتوي الطبقة العلوية على هيكل مرنان وأربعة مقاومات متكتلة. وُضعت صفيحة نحاسية، تعمل كسطح أرضي، على الجانب الخلفي للطبقة السفلية لتقليل خسائر الإرسال. تُفصل بين الطبقتين العلوية والسفلية طبقة هوائية رقيقة لتعزيز الامتصاص عند الترددات التشغيلية. الحجم الكلي لخلية وحدة MM هو ١٢×١٢×٤,٥٧ مم³، مع قياسات (٠,١٦ λ×٠,١٦ λ×٠,١٦ λ) عند أدنى تردد في طيف الامتصاص. صُممت معاوقة دخل خلية الوحدة بعناية لتتوافق مع معاوقة الفضاء الحر، مما يُسهّل امتصاص الطاقة الكهرومغناطيسية بكفاءة وإعادة توجيه مناسبة للأحمال المقاومة. يُقيّم أداء الممتص لزوايا استقطاب وسقوط مختلفة لكلٍّ من الوضعين الكهربائي المستعرض (TE) والمغناطيسي المستعرض (TM). تشير نتائج المحاكاة إلى أن الممتص المُدخل يحقق امتصاصًا واسع النطاق، متجاوزًا ٩٠٪ في نطاق الترددات من٤ جيجا هرتز إلى ٧ جيجا هرتز. من ناحية أخرى، تحقق خلية وحدة MM كفاءة حصاد تتجاوز ٨٠٪ في ظل السقوط الطبيعي، وتواصل إظهار أداء متميز عبر زوايا سقوط مختلفة لكلٍّ من الوضعين الكهربائي المستعرض والمغناطيسي المستعرض. تعمل هذه الدراسة على تحسين حصاد الطاقة المستند إلى MM بشكل كبير من خلال دمج الاستقبال بزاوية واسعة، وامتصاص النطاق العريض العالي، والحجم الصغير، وعدم حساسية الاستقطاب، مما يجعلها خيارًا مثاليًا لتزويد شبكات الاستشعار اللاسلكية (WSNs) بالطاقة.